



The sequential algorithm for combined state of charge and state of health estimation of lithium-ion battery based on active current injection

Ziyou Song^a, Jun Hou^b, Xuefeng Li^c, Xiaogang Wu^{c,*}, Xiaosong Hu^{d,**},
Heath Hofmann^b, Jing Sun^a

^a Department of Naval Architecture and Marine Engineering, University of Michigan, Ann Arbor, MI, 48109, USA

^b Department of Electrical Engineering and Computer Science, University of Michigan, Ann Arbor, MI, 48109, USA

^c College of Electrical and Electronics Engineering, Harbin University of Science and Technology, Harbin, 150080, China

^d Department of Automotive Engineering, Chongqing University, Chongqing, 400044, China

ARTICLE INFO

Article history:

Received 17 July 2019

Received in revised form

11 November 2019

Accepted 8 December 2019

Available online 10 December 2019

Keywords:

Lithium-ion battery

SoC/SoH estimation

Sequential algorithm

Active current injection

ABSTRACT

When the State of Charge, State of Health, and parameters of a Lithium-ion battery are estimated simultaneously, estimation accuracy is hard to be ensured due to uncertainties in the estimation process. A sequential algorithm, which uses frequency-scale separation and estimates parameters/states sequentially by injecting currents with different frequencies, is proposed in this paper to improve estimation performance. Specifically, by incorporating a high-pass filter, the parameters can be independently characterized by injecting high-frequency and medium-frequency currents, respectively. Using the estimated parameters, battery capacity and State of Charge can then be estimated concurrently. Experimental results show that the estimation accuracy of the proposed sequential algorithm is much better than the concurrent algorithm where all parameters/states are estimated simultaneously, and the computational cost can also be reduced. Finally, experiments are conducted at different temperatures to verify the effectiveness of the proposed algorithm for varying battery capacities.

© 2019 Elsevier Ltd. All rights reserved.

1. Introduction

Condition monitoring of lithium-ion batteries, such as the estimation of state of charge (SoC) and state of health (SoH), is essential for practical applications [1]. Estimation of SoC and SoH is generally intertwined with the estimation of battery parameters, which significantly vary with battery aging and changes in operating conditions [2] and are difficult to be adequately calibrated offline [3]. However, when all states/parameters are estimated simultaneously, substantial uncertainties are introduced in the estimation process [4], and the resulting inaccurate estimate of any parameter or state will dramatically impair the overall estimation performance. It has been proven that the estimation error of the multi-parameter estimation scenario (i.e., all states and parameters are estimated concurrently) is significantly increased when compared

to the single-parameter estimation scenario (i.e., only one parameter or state is estimated) [5]. Moreover, multi-parameter estimation imposes a critical constraint on the battery current profile since a persistently exciting (PE) input condition should be satisfied to ensure convergence of the estimated parameters and states [6]. Generally speaking, the PE condition requires one frequency component for every two estimated parameters [7]. Therefore, it is worthwhile to investigate new algorithms which can separate the estimation of battery states from parameters, and therefore improve estimation performance.

Model-based algorithms have been widely used for battery state estimation [8]. Commonly used models include the open circuit voltage (OCV) model [9], equivalent circuit model (ECM) [10], neural network model [11], and electrochemical model [12]. It is shown that multiple models can be adopted and switched online to improve SoC estimation performance [13]. A previous study has shown that the first-order ECM is an acceptable choice for lithium-ion batteries due to its adequate fidelity and low computational cost [14]. It is recently reported that the first-order ECM can be used for fresh cells and migrated to aged cells through the Bayes Monte

* Corresponding author.

** Corresponding author.

E-mail address: xgwu@hrbust.edu.cn (X. Wu).

Nomenclature			
a	OCV-SoC slope (V/%)	t_0	Start time (s)
b	Constant of the linearized OCV-SoC curve (V)	T_c	Time coefficient of the high-pass filter (s)
C_t	Capacitance of the RC pair (F)	T_s	Sampling time (s)
\mathbf{C}^x	Observation matrix for states	v_b	Battery terminal voltage (V)
\mathbf{C}^θ	Observation matrix for parameters	v_{bf}	Filtered battery terminal voltage (V)
i_b	Battery current (A)	v_c	Voltage over the RC pair (V)
i_{bf}	Filtered battery current (A)	\mathbf{v}_k	Measurement noise (V)
K_0-K_4	Coefficients of OCV-SoC curve	v_{oc}	Open circuit voltage of battery (V)
\mathbf{K}^x	Kalman gain for states	\mathbf{w}_k	Process noise for states
\mathbf{K}^θ	Kalman gain for parameters	\mathbf{X}_k	State vector
M	Current magnitude (A)	\mathbf{Y}_k	Output vector
Q_b	Battery capacity (Ah)	z	Battery SoC (%)
\mathbf{r}_k	Process noise for parameters	z_0	Battery initial SoC (%)
R_s	Ohmic resistance (Ω)	η	Columbic efficiency of battery (%)
\widehat{R}_s	Estimated ohmic resistance (Ω)	θ_k	Parameter vector
R_t	Resistance of the RC pair (Ω)	\mathbf{u}_k	Input vector
\widehat{R}_t	Estimated resistance of the RC pair (Ω)	Σ	Covariance matrix
s	Complex Laplace variable	τ	Time constant of the RC pair (s)
t	Time (s)	$\widehat{\tau}$	Estimated time constant of the RC pair (s)
		ω	Current speed (rad/s)

Carlo method [15]. The first-order ECM employed in this paper consists of an ohmic resistor R_s , an RC pair (R_t/C_t), and a DC voltage source v_{oc} , as shown in Fig. 1 [16]. In practical applications, these parameters, along with the SoC and SoH, should be estimated online [17].

Many algorithms have been developed and presented for SoC estimation. For example, coulomb counting is a basic open-loop method [18], which however is dramatically influenced by an inaccurate initial guess of SoC, and measurement noise [19]. The extended Kalman filter (EKF) is one of the most widely used methods [20]. In addition, unscented Kalman filters [21], sliding mode observers [22], particle filters [23], and H_∞ observers [24] have also been proposed in the literature. Similarly, for SoH, generally defined as the ratio of the remaining capacity to the original capacity [25], there are also many methodologies available for online implementation (e.g., adaptive EKF [26], multi-scale estimator [27], Box-Cox transformation [28], optimization-based method [29], co-estimation method [30]). We point out that the battery resistance can also indicate SoH in some applications [31], but in this paper SoH specifically corresponds to the available capacity of battery, despite the battery aging is not considered in the experimental validation. Since the estimation processes of battery

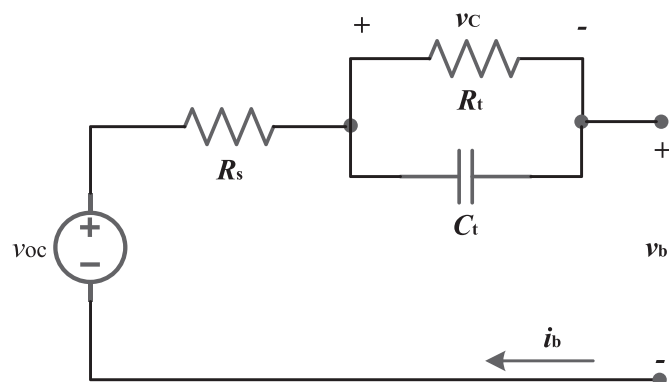


Fig. 1. The first-order equivalent circuit model for battery.

parameter, SoC, and SoH are coupled [32], the combined estimation has also been widely investigated [33]. Moreover, combined SoC/SoH estimation has been specifically investigated using the standard dual-extended Kalman filter (DEKF) [34]. The joint estimation of SoC and available energy of LiFePO4 batteries was conducted using particle filters [35]. Even though the estimation algorithm is important, scholars have also focused on shaping the input-output data; i.e., the battery current and voltage, to further improve estimation accuracy [36].

An over-actuated system (e.g., hybrid energy storage system) offers an additional degree of freedom which provides the opportunity to inject desired input signals for identification objectives while simultaneously achieving control objectives [37]. To improve estimation performance, a sequential algorithm is proposed in this paper to estimate the parameters/states sequentially through active current injection. The first-order ECM is analyzed first to exploit frequency-scale separation of different dynamics associated with different parameters and states. Specifically, the battery dynamics is governed by the initial SoC, the SoC variation, the ohmic resistance R_s , and the RC pair. It can be found that the initial SoC dynamics can be removed from the battery voltage dynamics with a high-pass filter. In addition, simulation results show that for the 18650 Lithium-ion battery studied in this work, SoC variations can be neglected as long as the battery current frequency is not extremely low (i.e., below 0.001 Hz), and the ECM dynamic behavior is dominated by the resistance R_s when the battery current frequency is high (i.e., above 0.1 Hz). Consequently, in Step #1 the proposed sequential algorithm estimates the ohmic resistance R_s independently by injecting a high-frequency current and incorporating a high-pass filter, since the RC pair can be regarded as a short-circuit under these conditions. In Step #2, based on the estimated R_s , the RC pair can be characterized (i.e., the diffusion resistance R_t and the time constant τ) by injecting a medium-frequency current. Finally, in Step #3, the battery capacity and SoC can be estimated concurrently based on the previously estimated parameters. The EKF is adopted in Steps #1 and #2 to estimate battery parameters, and a DEKF is adopted in Step #3 to estimate the battery SoC and SoH. The experimental results verify the effectiveness of the proposed sequential algorithm, which

significantly increases the estimation accuracy when compared to the case where all parameters/states are estimated simultaneously.

The rest of the paper is organized as follows. In Section 2, the parameter/state estimation problem for Lithium-ion batteries is formulated and analyzed. In Section 3, the sequential algorithm is proposed. In Section 4, experimental results are provided for validation. Conclusions are given in Section 5.

2. System description

2.1. The first-order equivalent circuit model

Defining the battery terminal voltage as v_b and the battery current as i_b (positive for discharging and negative for charging), as shown in Fig. 1, the ECM dynamics are derived as follows:

$$\begin{cases} \dot{v}_C = -\frac{1}{C_t R_t} v_C + \frac{1}{C_t} i_b \\ v_b = v_{OC} - R_s i_b - v_C \end{cases} \quad (1)$$

where v_C is the RC pair voltage and v_{OC} denotes the OCV. The OCV-SoC relation is given by Ref. [38].

$$v_{OC}(z) = K_0 - \frac{K_1}{z} - K_2 z + K_3 \ln(z) + K_4 \ln(1-z), \quad (2)$$

where K_{0-4} are the constant coefficients and z represents the normalized SoC, and the SoC dynamic is given as [39].

$$z = z_0 - \int_{t_0}^t \frac{\eta}{Q_b} i_b(t) dt, \quad (3)$$

where z_0 , η , t_0 , and Q_b represent the initial SoC, the charging/discharging efficiency, the start time, and the battery capacity, respectively. To simplify the analysis, the OCV-SoC relationship is linearized as [40].

$$v_{OC}(t) = a \left(z_0 - \int_{t_0}^t \frac{\eta i_b(v)}{Q_b} dv \right) + b, \quad (4)$$

where a and b are the corresponding coefficients. Note that this linearized relationship is only used in the analysis, while in the estimation process the nonlinear relationship shown in Eq. (2) is used. The coefficients K_{0-4} in the OCV-SoC relationship are acquired under 20 °C for a fresh cell (i.e., the SoH is 100%) in this paper. For simplification, it is assumed that K_{0-4} do not change under different SoH levels, as verified in existing literature [41,42]. However, we note that the above assumption cannot be guaranteed for all battery chemistries. If coefficients K_{0-4} are significantly influenced by battery degradation, the proposed sequential algorithm may encounter challenges, as almost all existing estimation algorithms do. In addition, ECM parameters, including R_s , R_t , and τ , are significantly influenced by battery degradation and operating conditions, and are therefore difficult to calibrate for all practical scenarios [26]. Especially, the influence of degradation on the battery characteristics is almost impossible to be entirely investigated offline [43]. As a result, battery parameters should be estimated online along with battery SoC and SoH. Since battery parameters vary more slowly than the battery SoC [26], two assumptions are made in the estimation process:

- 1) The initial value of v_C is 0, and
- 2) The parameters of R_s , R_t , and τ are assumed to be constant.

Under these assumptions, based on Eqs. (1) and (4), the transfer function from i_b to v_b is obtained.

$$v_b(s) = \frac{az_0}{s} + \frac{b}{s} - \frac{a}{s} \frac{\eta}{Q_b} i_b(s) - R_s i_b(s) - \frac{R_t}{1 + \tau s} i_b(s), \quad (5)$$

where s is the complex Laplace variable. There are therefore three parameters (i.e., R_s , R_t , and C_t) and two states (i.e., z_0 and Q_b) in Eq. (5) to be estimated.

2.2. The analysis of the first-order ECM dynamics

As shown in Eq. (5), the battery terminal voltage dynamics include four parts. The first part ($a \cdot z_0/s + b/s$) is constant and related to the initial SoC. The second ($-a \cdot \eta \cdot i_b(s)/s \cdot Q_b$) is related to the SoC variation and is significantly influenced by the battery capacity. The third ($-R_s \cdot i_b(s)$) is related to the ohmic resistance, and the fourth ($-R_t \cdot i_b(s)/(1 + \tau \cdot s)$) is related to the RC pair. Since the first part is constant, it can be removed by a high-pass filter. A first-order high-pass filter is applied to Eq. (5), which yields:

$$v_{bf}(s) = \frac{(az_0 + b)T_c}{1 + T_c s} - \frac{a}{s} \frac{\eta}{Q_b} i_{bf}(s) - R_s i_{bf}(s) - \frac{R_t}{1 + \tau s} i_{bf}(s), \quad (6)$$

where

$$\begin{cases} v_{bf}(s) = \frac{T_c s}{1 + T_c s} v_b(s) \\ i_{bf}(s) = \frac{T_c s}{1 + T_c s} i_b(s) \end{cases},$$

T_c is the time coefficient of the high-pass filter, and v_{bf} and i_{bf} are the filtered battery voltage and current, respectively. The dynamics of the filtered system can then be presented in the time domain through the inverse Laplace transform. The effects of the initial SoC are given as

$$L^{-1} \left\{ \frac{(az_0 + b)T_c}{1 + T_c s} \right\} = (az_0 + b) e^{-\frac{t}{T_c}}, \quad (7)$$

which will decay exponentially over time, at the rate defined by T_c . To evaluate the effects of the high-pass filter on separating the battery dynamics, we consider Samsung 18650 Lithium-ion batteries. The parameters of an 18650 Lithium-ion battery are specified in Table 1. The coefficients K_{0-4} of the OCV-SoC relationship for the adopted cell are 2.6031, 0.0674, -1.527, 0.6265, and -0.0297, respectively. The initial SoC dynamics vanish more quickly as T_c decreases (i.e., the cut-off frequency increases). The initial SoC dynamics are removed from the battery terminal voltage after ~6 min when T_c is 80s. Therefore the initial SoC can be neglected in the filtered system and it will not influence the estimation of the other parameters/states. As shown in Eq. (6), except for the initial

Table 1
Specifications for the Samsung 18650 battery cell.

Parameter	Value
Nominal Voltage (V)	3.63
Cell Capacity (Ah)	2.47
Discharge/Charge Coulombic Efficiency η (%)	98
OCV-SoC slope a (mV/100%)	-8.845
Standard Deviation of Voltage Measurement Noise σ_v (mV)	20
Battery Current Amplitude M (A)	1
Ohmic Resistance R_s (m Ω)	~100
Diffusion Resistance R_t (m Ω)	~30
Time Constant τ (s)	~15

SoC response, the other responses are significantly influenced by the filtered current i_{bf} . To quantify the influence of the current's frequency on the voltage dynamics a sinusoidal current is considered in this paper:

$$\begin{cases} i_b(t) = M \cos(\omega t) \\ i_b(s) = \frac{Ms}{s^2 + \omega^2} \end{cases}, \quad (8)$$

where M and ω are the current magnitude and frequency, respectively.

To clearly show the influence of current frequency, the battery voltage responses when the current frequency is 0.4 Hz, 0.004 Hz, and 0.0004 Hz are shown in Fig. 2, where T_c is fixed at 80s. When the current frequency is 0.4 Hz, as shown in Fig. 2 (a), the battery terminal voltage is governed by its ohmic resistance component, and the SoC variation component as well as the RC pair component can be neglected. The RC pair can be regarded as a short circuit when the current frequency is sufficiently high. In addition, the SoC variation component is small because high-frequency current does not induce a significant change in the battery SoC. This means that, based on the filtered signals, R_s can be estimated independently by injecting high-frequency current regardless of the other parameters. As shown in Fig. 2 (b), the RC pair component is comparable with the ohmic resistance component when the current frequency decreases to 0.004 Hz, while the SoC variation dynamics can still be neglected. Assuming that the parameters do not change quickly [26], the estimated R_s can be used to estimate R_t and τ when the current frequency is around 0.004 Hz (i.e., medium-frequency current). As the current frequency further decreases to 0.0004 Hz, as shown in Fig. 2 (c), none of three components can be neglected. The analysis presented above indicates the possibility of separating battery dynamics in the frequency domain by injecting the current with different frequencies, and therefore informs the sequential estimation algorithm proposed in the next section.

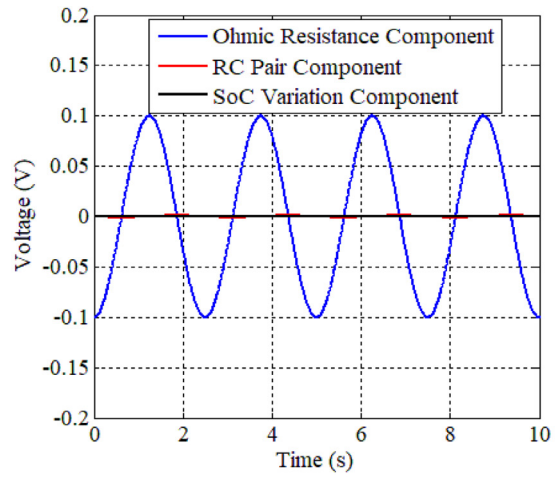
3. The sequential algorithm for combined SoC and SoH estimation

To reduce uncertainty in the estimation process and therefore increase estimation accuracy, a sequential algorithm is proposed in this paper, as shown in Fig. 3. A high-pass filter is used to block the constant initial SoC component, and a high-frequency current is injected to estimate the ohmic resistance R_s . Using the estimated R_s , a medium-frequency current is injected to estimate the diffusion resistance R_t and the time constant τ . After obtaining the estimated R_s , R_t , and τ , the SoC and SoH can be estimated finally.

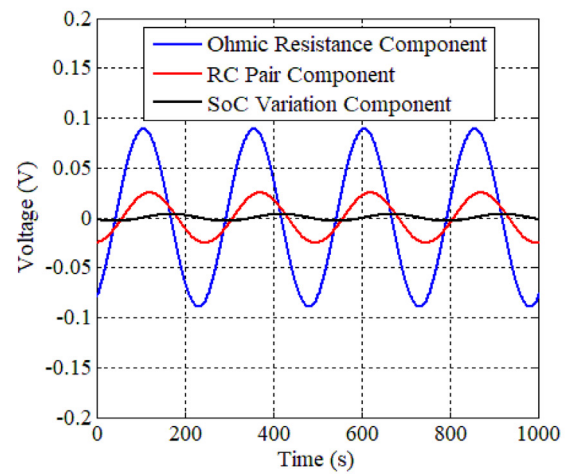
The sequential algorithm, which estimates the battery parameters and states separately, can reduce computational cost when compared to the case when all states and parameters are estimated simultaneously [44]. More importantly, the sequential algorithm can improve estimation accuracy since it exploits frequency separation and eliminates the interactions of parameter and state estimation [36]. Three steps are involved in the sequential estimation, and the associated algorithms are presented herein.

3.1. A review of EKF and DEKF

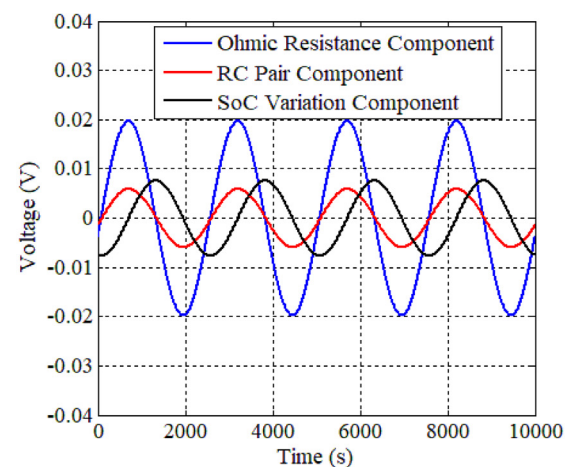
An EKF is used in Steps #1 and #2 of the sequential algorithm to estimate the battery parameters. The EKF determines the optimal feedback gain to suppress both process noise and measurement noise [45]. The general discrete time state-space equation can be illustrated as



(a) ω is 0.4Hz



(b) ω is 0.004Hz



(c) ω is 0.0004Hz

Fig. 2. The battery voltage component due to various current frequencies.

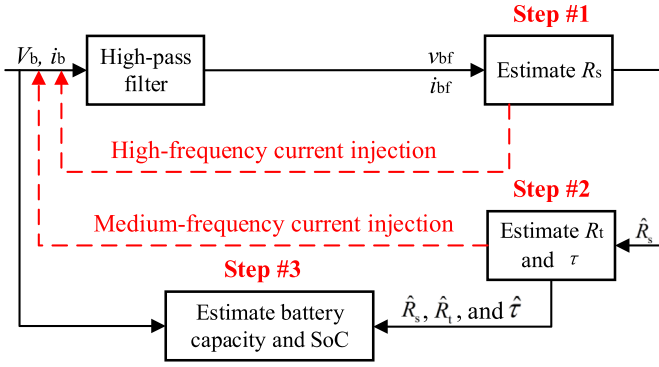


Fig. 3. The flowchart of the sequential algorithm.

$$\begin{cases} \boldsymbol{\theta}_{k+1} = \boldsymbol{\theta}_k + \mathbf{r}_k \\ \mathbf{X}_{k+1} = \mathbf{H}(\mathbf{X}_k, \boldsymbol{\theta}_k, \mathbf{u}_k) + \mathbf{w}_k \\ \mathbf{Y}_{k+1} = \mathbf{G}(\mathbf{X}_k, \boldsymbol{\theta}_k, \mathbf{u}_k) + \mathbf{v}_k \end{cases} \quad (9)$$

where k is the time index, \mathbf{X}_k is the state vector, $\boldsymbol{\theta}_k$ is the parameter vector, \mathbf{u}_k is the input vector, \mathbf{Y}_k is the output vector, \mathbf{r}_k is the process noise for the parameters, \mathbf{w}_k is the process noise for the states, and \mathbf{v}_k is the measurement noise. In Steps #1 and #2, only the battery parameters are estimated, and the battery states are not involved. The calculation process of the EKF is summarized in Table 2. In Step #3, combined SoC and SoH estimation is conducted based on the original system. We point out that the high-order OCV-SoC relationship (see Eq. (2)) is used to estimate SoC and SoH. The remaining battery capacity, which is also one of the battery parameters, is estimated to determine the SoH.

As a result, both the parameter (i.e., battery capacity) and the state (i.e., SoC) need to be estimated in Step #3. The DEKF method is a commonly used technique to simultaneously estimate states and parameters [46]. The DEKF adopts two EKFs run in parallel and estimates the state/parameter using each other's latest updates [47]. Based on Eq. (9), the detailed algorithms of the DEKF is specified in Table 3.

Table 2
EKF algorithm.

Initialization:

$$\begin{cases} \hat{\boldsymbol{\theta}}_0 = E[\boldsymbol{\theta}_0] \\ \sum_{\boldsymbol{\theta}_0} = E[(\boldsymbol{\theta}_0 - \hat{\boldsymbol{\theta}}_0)(\boldsymbol{\theta}_0 - \hat{\boldsymbol{\theta}}_0)^T] \end{cases} \quad (10)$$

where $\sum_{\boldsymbol{\theta}_0}$ is the covariance matrix of parameter estimation error.

Parameter prediction:

$$\begin{cases} \hat{\boldsymbol{\theta}}_k^- = \hat{\boldsymbol{\theta}}_{k-1} \\ \sum_{\boldsymbol{\theta}_k}^- = \sum_{\boldsymbol{\theta}_{k-1}} + \sum_{\mathbf{r}_{k-1}} \end{cases} \quad (11)$$

where $\sum_{\mathbf{r}_{k-1}}$ is the covariance matrix of process noise.

Parameter update:

$$\begin{cases} \mathbf{K}_k^{\boldsymbol{\theta}} = \sum_{\boldsymbol{\theta}_{k-1}}^- (\mathbf{C}_{k-1}^{\boldsymbol{\theta}})^T [(\mathbf{C}_{k-1}^{\boldsymbol{\theta}}) \sum_{\boldsymbol{\theta}_{k-1}}^- (\mathbf{C}_{k-1}^{\boldsymbol{\theta}})^T + \sum_{\mathbf{v}_{k-1}}^-]^{-1} \\ \hat{\boldsymbol{\theta}}_k = \hat{\boldsymbol{\theta}}_k^- + \mathbf{K}_k^{\boldsymbol{\theta}} [\mathbf{Y}_k - \mathbf{G}(\mathbf{X}_{k-1}, \hat{\boldsymbol{\theta}}_k^-, \mathbf{u}_k)] \\ \sum_{\boldsymbol{\theta}_k} = (\mathbf{I} - \mathbf{K}_k^{\boldsymbol{\theta}} \mathbf{C}_{k-1}^{\boldsymbol{\theta}}) \sum_{\boldsymbol{\theta}_{k-1}}^- \end{cases} \quad (12)$$

$$\text{where } \mathbf{C}_{k-1}^{\boldsymbol{\theta}} = \frac{\partial \mathbf{G}(\mathbf{X}_{k-1}, \boldsymbol{\theta}, \mathbf{u}_k)}{\partial \boldsymbol{\theta}} \Big|_{\boldsymbol{\theta} = \hat{\boldsymbol{\theta}}_k^-}.$$

Table 3
DEKF algorithm.

Initialization:

$$\begin{cases} \hat{\boldsymbol{\theta}}_0 = E[\boldsymbol{\theta}_0] \\ \sum_{\boldsymbol{\theta}_0} = E[(\boldsymbol{\theta}_0 - \hat{\boldsymbol{\theta}}_0)(\boldsymbol{\theta}_0 - \hat{\boldsymbol{\theta}}_0)^T] \\ \hat{\mathbf{X}}_0 = E[\mathbf{X}_0] \\ \sum_{\mathbf{X}_0} = E[(\mathbf{X}_0 - \hat{\mathbf{X}}_0)(\mathbf{X}_0 - \hat{\mathbf{X}}_0)^T] \end{cases} \quad (13)$$

where $\sum_{\mathbf{X}_0}$ is the covariance matrix of state estimation error.

Parameter prediction:

$$\begin{cases} \hat{\boldsymbol{\theta}}_k^- = \hat{\boldsymbol{\theta}}_{k-1} \\ \sum_{\boldsymbol{\theta}_k}^- = \sum_{\boldsymbol{\theta}_{k-1}} + \sum_{\mathbf{r}_{k-1}} \end{cases} \quad (14)$$

State prediction:

$$\begin{cases} \hat{\mathbf{X}}_k^- = \mathbf{H}(\hat{\mathbf{X}}_{k-1}, \hat{\boldsymbol{\theta}}_k^-, \mathbf{u}_k) \\ \sum_{\mathbf{X}_k}^- = \mathbf{A}_k \sum_{\mathbf{X}_{k-1}} \mathbf{A}_k^T + \sum_{\mathbf{w}_k} \end{cases} \quad (15)$$

$$\text{where } \mathbf{A}_k = \frac{\partial \mathbf{H}(\mathbf{X}, \hat{\boldsymbol{\theta}}_k^-, \mathbf{u}_k)}{\partial \mathbf{X}} \Big|_{\mathbf{X} = \hat{\mathbf{X}}_k^-}.$$

State update:

$$\begin{cases} \mathbf{K}_k^{\mathbf{X}} = \sum_{\mathbf{X}_k}^- (\mathbf{C}_k^{\mathbf{X}})^T [(\mathbf{C}_k^{\mathbf{X}}) \sum_{\mathbf{X}_k}^- (\mathbf{C}_k^{\mathbf{X}})^T + \sum_{\mathbf{v}_k}^-]^{-1} \\ \hat{\mathbf{X}}_k = \hat{\mathbf{X}}_k^- + \mathbf{K}_k^{\mathbf{X}} [\mathbf{Y}_k - \mathbf{G}(\hat{\mathbf{X}}_k^-, \hat{\boldsymbol{\theta}}_k^-, \mathbf{u}_k)] \\ \sum_{\mathbf{X}_k} = (\mathbf{I} - \mathbf{K}_k^{\mathbf{X}} \mathbf{C}_k^{\mathbf{X}}) \sum_{\mathbf{X}_k}^- \end{cases} \quad (16)$$

$$\text{where } \mathbf{C}_k^{\mathbf{X}} = \frac{\partial \mathbf{G}(\mathbf{X}, \hat{\boldsymbol{\theta}}_k^-, \mathbf{u}_k)}{\partial \mathbf{X}} \Big|_{\mathbf{X} = \hat{\mathbf{X}}_k^-}.$$

Parameter update:

$$\begin{cases} \mathbf{K}_k^{\boldsymbol{\theta}} = \sum_{\boldsymbol{\theta}_k}^- (\mathbf{C}_k^{\boldsymbol{\theta}})^T [(\mathbf{C}_k^{\boldsymbol{\theta}}) \sum_{\boldsymbol{\theta}_k}^- (\mathbf{C}_k^{\boldsymbol{\theta}})^T + \sum_{\mathbf{v}_k}^-]^{-1} \\ \hat{\boldsymbol{\theta}}_k = \hat{\boldsymbol{\theta}}_k^- + \mathbf{K}_k^{\boldsymbol{\theta}} [\mathbf{Y}_k - \mathbf{G}(\hat{\mathbf{X}}_k^-, \hat{\boldsymbol{\theta}}_k^-, \mathbf{u}_k)] \\ \sum_{\boldsymbol{\theta}_k} = (\mathbf{I} - \mathbf{K}_k^{\boldsymbol{\theta}} \mathbf{C}_k^{\boldsymbol{\theta}}) \sum_{\boldsymbol{\theta}_k}^- \end{cases} \quad (17)$$

$$\text{where } \mathbf{C}_k^{\boldsymbol{\theta}} = \frac{d\mathbf{G}(\hat{\mathbf{X}}_k^-, \boldsymbol{\theta}, \mathbf{u}_k)}{d\boldsymbol{\theta}} \Big|_{\boldsymbol{\theta} = \hat{\boldsymbol{\theta}}_k^-}.$$

3.2. The sequential algorithm

Incorporating the algorithms described in Section 3.1, the sequential parameter and SoC/SoH estimation approach is formulated in 3 steps.

Step #1: The first step of the sequential algorithm is estimating the ohmic resistance by using a high-pass filter and injecting high-frequency current. Based on Eq. (6), the battery terminal voltage can be simplified as

$$v_{\text{bf}}(s) = -R_s i_{\text{bf}}(s) \quad (18)$$

Therefore, the discrete time state-space equation (9) for estimating the ohmic resistance R_s using the EKF can be given as

$$\begin{cases} R_s(k) = R_s(k-1) + r_k \\ v_{\text{bf}}(k) = -R_s i_{\text{bf}}(k) + v_k \end{cases} \quad (19)$$

Step #2: When the medium-frequency current is injected, the battery terminal voltage is governed by ohmic resistance dynamics and RC pair dynamics, so Eq. (6) can be simplified as

$$v_{\text{bf}}(s) = -R_s i_{\text{bf}}(s) - \frac{R_t}{1 + \tau s} i_{\text{bf}}(s) \quad (20)$$

The estimated ohmic resistance obtained in Step #1 is then used in Step #2, and the bilinear transformation is used to discretize Eq. (20). Consequently, the discrete time state-space equation (11) for estimating R_t and τ is given as

$$\begin{cases} \boldsymbol{\theta}_2(k) = \boldsymbol{\theta}_2(k-1) + \mathbf{r}_k \\ v_{\text{bf}}(k) = -\widehat{R}_s(k) i_{\text{bf}}(k) - R_t i_2(k) + \mathbf{v}_k \end{cases} \quad (21)$$

where

$$\begin{cases} \boldsymbol{\theta}_2(k) = [R_t(k) \quad \tau(k)]^T \\ i_2(k) = \frac{T_s}{T_s + 2\tau} [i_{\text{bf}}(k) + i_{\text{bf}}(k-1)] - \frac{T_s - 2\tau}{T_s + 2\tau} i_2(k-1) \end{cases},$$

and T_s is the sampling period (i.e., 1s).

Step #3: Given that R_s , R_t , and τ are estimated in Steps #1 and #2, the SoC and SoH can be simultaneously estimated in Step #3. Based on Eqs. (1)–(3), the discrete time state-space equation for estimating the SoC and SoH estimation is shown to be

$$\begin{cases} Q_b(k) = Q_b(k-1) + r_k \\ \mathbf{X}_3(k) = \begin{bmatrix} e^{-\frac{T_s}{\tau}} & 0 \\ 0 & 1 \end{bmatrix} \mathbf{X}_3(k-1) + \begin{bmatrix} \widehat{R}_t \left(1 - e^{-\frac{T_s}{\tau}}\right) \\ -\frac{\eta T_s}{Q_b} \end{bmatrix} i_b(k), \\ v_b(k) = \text{OCV}(z(k)) - v_c(k) - \widehat{R}_s(k) i_b(k) \end{cases} \quad (22)$$

where

$$\mathbf{X}_3(k) = [v_c(k) \quad z(k)]^T$$

As shown in Eq. (22), the voltage of the RC pair v_c is also estimated for better performance [2], and the DEKF presented in Section 3.1 is adopted. Since SoC and SoH are estimated together, an inaccurate estimation of either SoC or SoH will influence the other. However, the estimation accuracy can still be significantly improved for the proposed algorithm, since less uncertainty is involved when compared to the case where all battery parameters/states are estimated simultaneously.

For different battery cells, which are manufactured by different companies or have different chemistries, the battery parameters may vary significantly. As a result, the frequency of the injected current and the cut-off frequency of the high-pass filter should be adapted to specific battery cells. At any rate, the proposed sequential algorithm is a general method for battery parameter/state estimation.

4. Experimental results

Experimental testing is focused on an 18650 Lithium-ion battery (see Table 1 for detailed information). In the experiments, error

caused by ECM inaccuracy is introduced. An Arbin battery test system (BT2000) was used in the following experiments [48]. The initial SoC is 80% for all four experiments, and they are illustrated as follows.

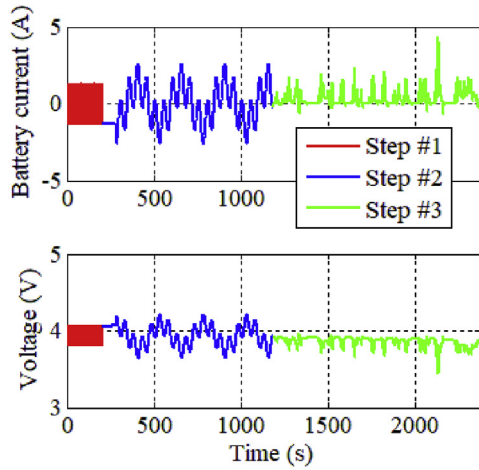
Experiment #1: Validation of the sequential algorithm at 20 °C. In Experiment #1, the initial guesses of the estimated parameters are $[\widehat{R}_s(0) \quad \widehat{R}_t(0) \quad \widehat{\tau}(0) \quad \widehat{Q}_b(0)] = [0.02 \quad 0.03 \quad 15 \quad 2]$, and the initial values of estimated SoC and v_c are 50% and 0 V, respectively. As shown in Fig. 4(a), in Step #1 a 0.5 Hz sinusoidal current with amplitude of 0.5C is injected and the first-order butterworth high-pass filter has a 3 dB bandwidth of 0.05 Hz. As shown in Fig. 2 (a), the adopted current frequency (i.e., 0.5 Hz) can extract the battery voltage component governed by the ohmic resistance and the other components (RC pair and SoC components) are negligible. Therefore, the ohmic resistance can be accurately estimated given that the uncertainty in the estimation process is reduced. The estimation result of R_s is shown in Fig. 4(b), which indicates that the estimated value can accurately track the actual value, which is obtained from the HPPC test.

In Step #2 a 0.02 Hz sinusoidal current with amplitude of 0.5C is added onto a base current (0.004 Hz sinusoidal current with amplitude of 0.5C) and the first-order butterworth high-pass filter has 3 dB bandwidth of 0.002 Hz. As shown in Fig. 2 (b), the current frequencies in Step #2 (i.e., 0.02 Hz and 0.004 Hz) can separate the components corresponding to the ohmic resistance and the RC pair from the one related to the SoC variation. Therefore, the RC pair parameters can be accurately estimated based on the estimation result in Step #1 (i.e., estimated ohmic resistance). As shown in Fig. 4(c), the estimated parameters can track the actual values for R_t and τ , but there is a slight static error in the R_t estimation result. Therefore, the first-order ECM has limitations representing the studied 18650 Lithium-ion battery, as the RC pair parameters are hard to estimate. Since the sampling frequency in Step #1 is high, we need to manually control the Arbin test system and switch to Step #2 in the experiment. As a result, there is a transient period from 200s to 287s, which is shown in Fig. 4(a). The estimation process of Step #2 is from 288s to 1187s, which includes a hold-up time of 400s to avoid initial SoC dynamics. Step #3 starts from 1200s.

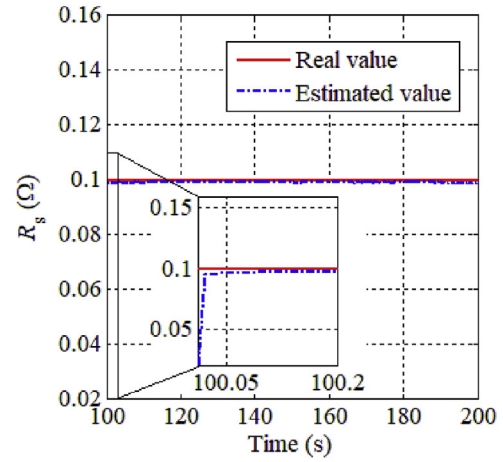
The estimated R_s , R_t , and τ are used in Step #3 to estimate SoC and SoH simultaneously. A scaled bus driving cycle is used in Step #3 to represent a practical profile for batteries. As shown in Fig. 4(d), the SoC estimation performance is satisfactory and the estimation error is below 1% under a significant initial error (30%). As shown in Fig. 4(e), the estimated battery capacity accurately tracks the actual value obtained from the static capacity test after 1800s, and there is no significant error after convergence. The estimated voltage shown in Fig. 4(f) tracks the actual terminal value well. As a result, the effectiveness of the proposed sequential algorithm is verified experimentally.

Experiment #2: Validation of the sequential algorithm at 40 °C. In Experiment #2, the temperature is increased to 40 °C, and the battery parameters slightly change when compared to those of 20 °C according to the battery static capacity test [49]. Especially, the battery capacity increases from 2.47Ah to 2.62Ah. The initial guesses of the estimated parameters and states are similar to those in Experiment #1, as the parameters do not significantly change when the temperature increases from 20 °C to 40 °C.

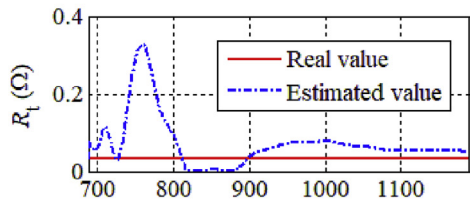
The same current profile, as shown in Fig. 4(a), as well as the same high-pass filters are used. As shown in Fig. 5(a) and (b), the parameter estimation performance is satisfactory and similar to the results of Experiment #1. The consistent results verify the effectiveness of the proposed sequential algorithm on battery parameter estimation. The SoC estimation error is less than 1% when the initial guess error is 30%, as shown in Fig. 5(c). For the battery capacity



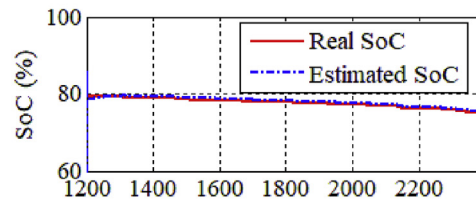
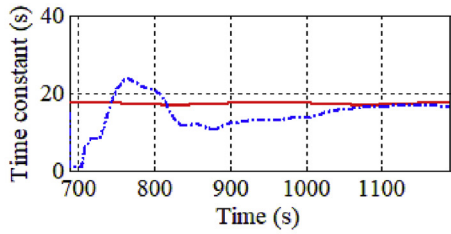
(a) The battery current profile



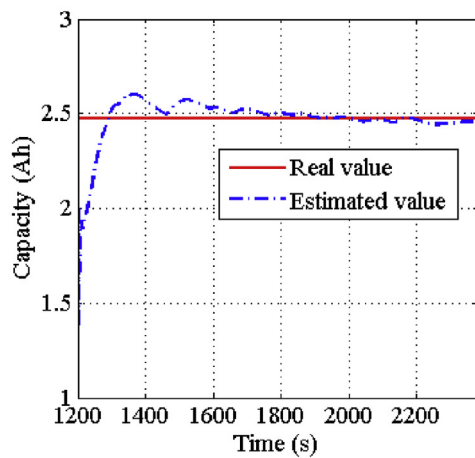
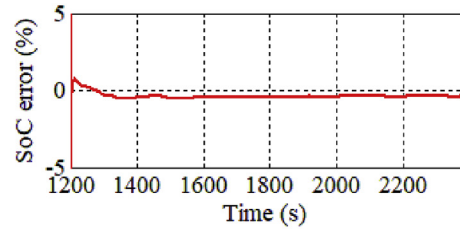
(b) R_s estimation result (Step #1)



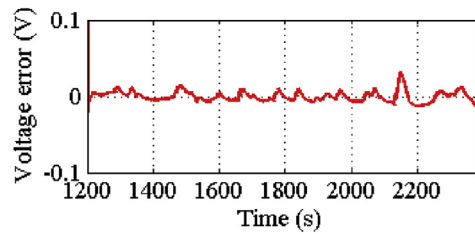
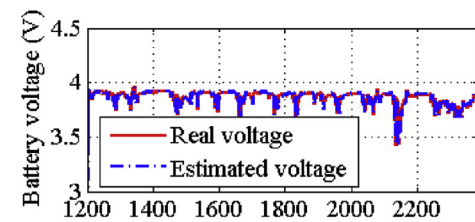
(c) R_i and τ estimation result (Step #2)



(d) SoC estimation result (Step #3)

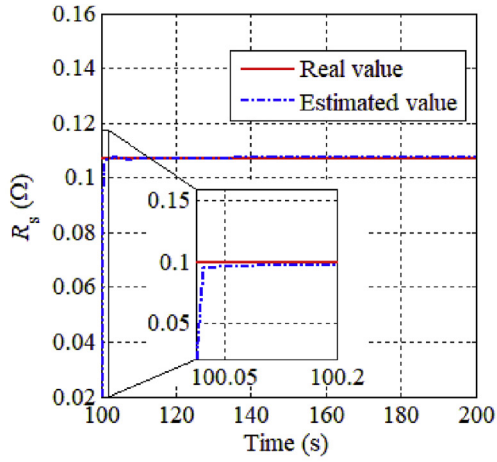


(e) Q_b estimation result (Step #3)

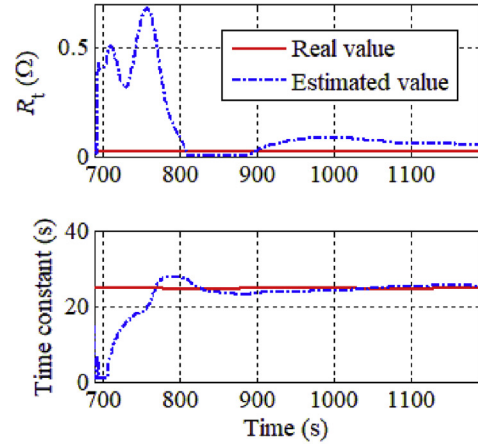


(f) v_b estimation result (Step #3)

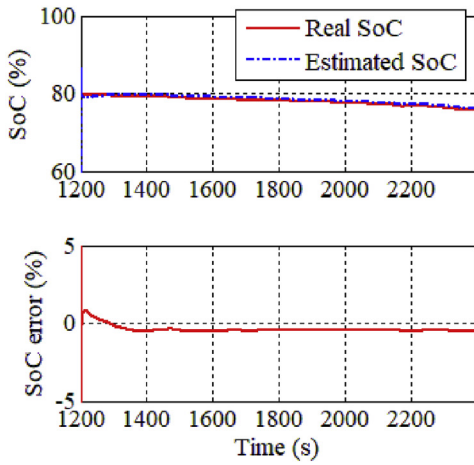
Fig. 4. Experimental results at 20 °C.



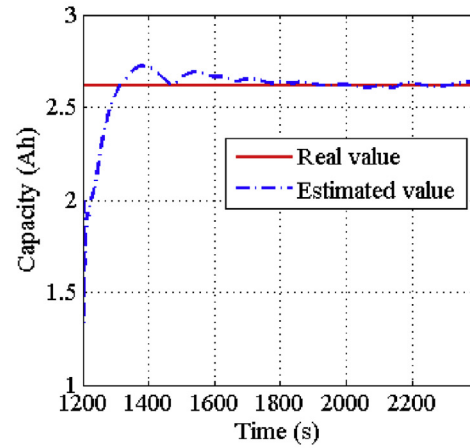
(a) R_s estimation result (Step #1)



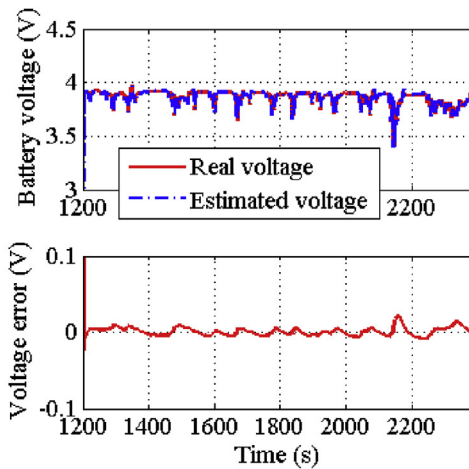
(b) R_i and τ estimation result (Step #2)



(c) SoC estimation result (Step #3)

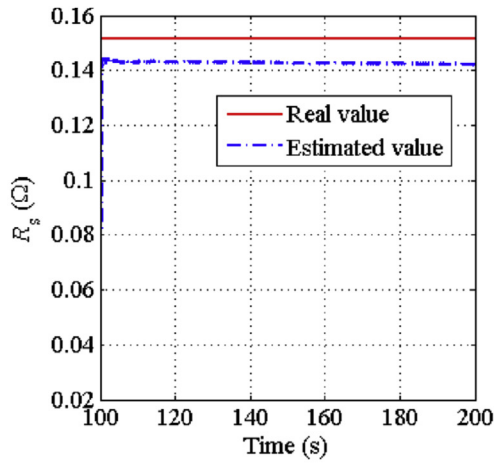


(d) Q_b estimation result (Step #3)

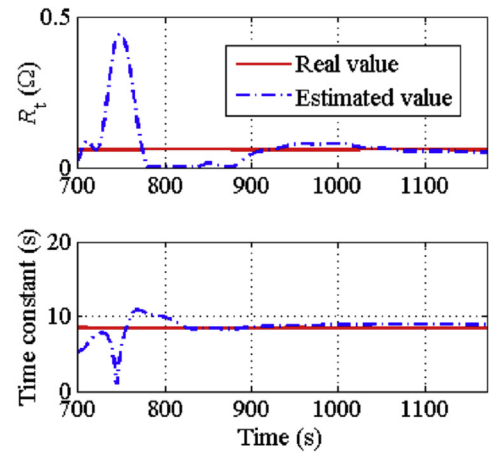


(e) v_b estimation result (Step #3)

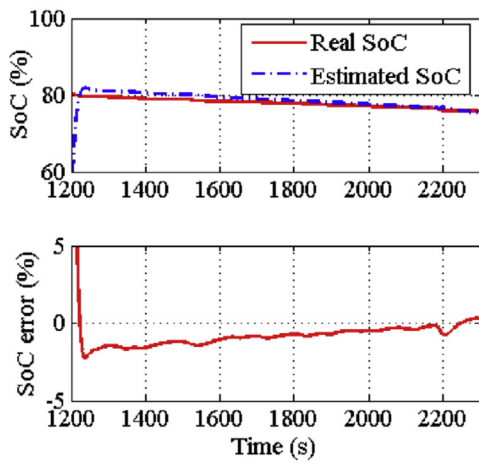
Fig. 5. Experimental results at 40 °C.



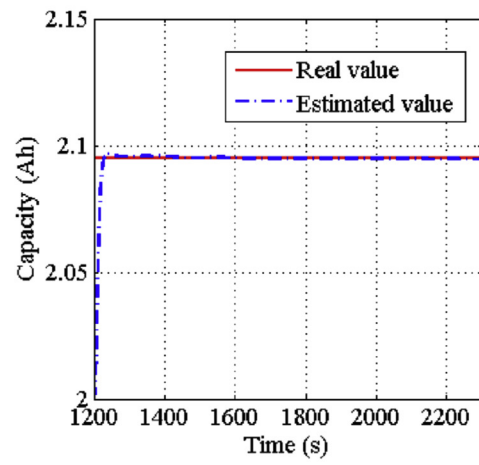
(a) R_s estimation result (Step #1)



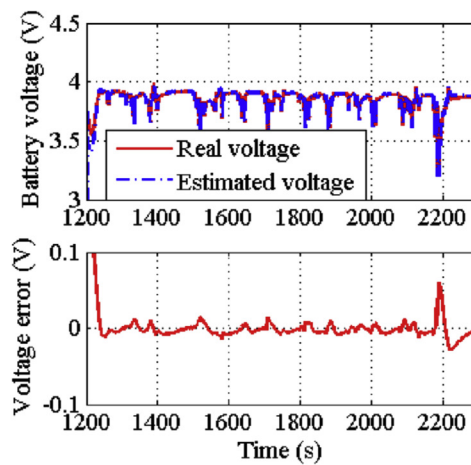
(b) R_t and τ estimation result (Step #2)



(c) SoC estimation result (Step #3)



(d) Q_b estimation result (Step #3)



(e) v_b estimation result (Step #3)

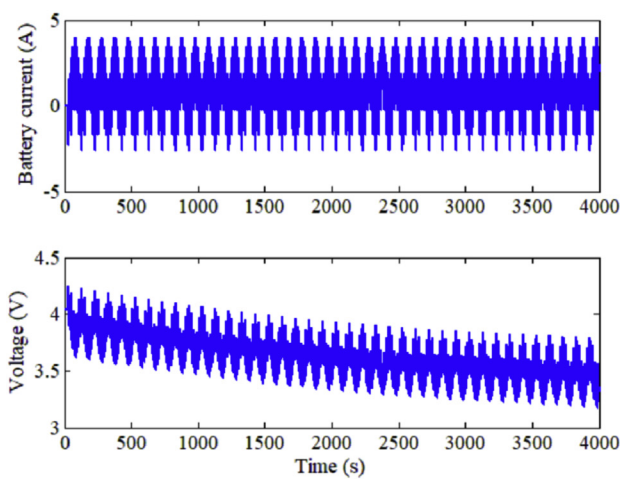
Fig. 6. Experimental results at 0 °C.

(i.e., SoH), the convergence time is about 600s, and no significant static error exists after convergence, as shown in Fig. 5(d). Therefore, the sequential algorithm can accurately co-estimate the battery states (i.e., SoC and SoH) at high-temperature conditions.

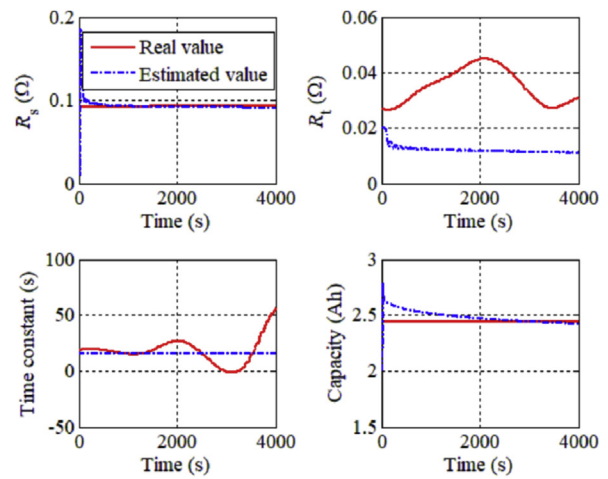
Experiment #3: Validation of the sequential algorithm at 0 °C. In Experiment #3, the temperature is decreased to 0 °C, since the battery state estimation is challenging at low temperatures. The initial guesses of the estimated parameters are $[\hat{R}_s(0) \hat{R}_t(0) \hat{\tau}(0) \hat{Q}_b(0)] = [0.02 \ 0.03 \ 5 \ 2]$. Note that all battery parameters significantly vary due to the temperature change, especially, the ohmic resistance increases by up to 60% when the temperature decreases from 20 °C to 0 °C. In addition, a static error, which does not exist in Experiment #1 and #2, can be found in the estimation result of R_s at 0 °C, as shown in Fig. 6 (a). We point out that in this paper the “real value” of R_s denotes the parameter calibrated in the HPPC test. Given that R_s is calculated based on the voltage drop corresponding to the pulse current, the “real value” of R_s indicates the high-frequency response of battery (i.e., 1s resistance), while in Step #1 the estimated R_s corresponds to the battery

response at 0.5 Hz. Therefore, the estimated and the actual values of R_s reflect the battery characteristics under different frequencies. The electrochemical impedance spectroscopy (EIS) measurement provided in Ref. [50] shows that the variation of battery EIS (from 0.5 Hz to 1 Hz) becomes significant with decreasing temperature, especially for the high SoC range (e.g., 80% SoC in this study). This is the reason for which the static estimation error of R_s can be found at 0 °C. We point out that the “real values” for all parameters are relatively accurate since they only represent the battery response under the HPPC test.

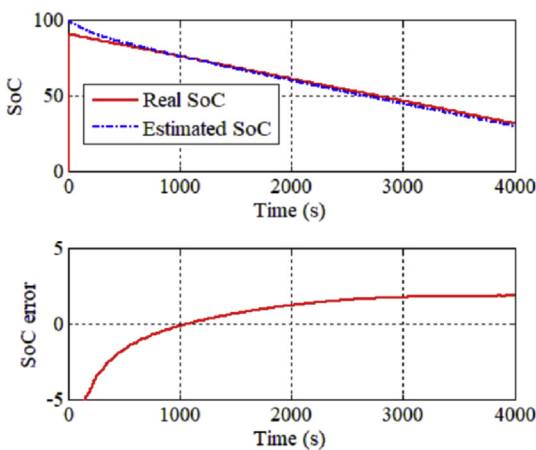
As shown in Fig. 6(b), the RC pair parameters are estimated accurately and no significant estimation errors are found. Similarly, the SoC estimation error is small and less than 1% given the initial guess error of 30%, as shown in Fig. 6(c). The battery capacity decreases to 2.10Ah when the temperature decreases to 0 °C and it can be accurately estimated along the entire process of Step #3, as shown in Fig. 6(d). As a result, the terminal voltage can be accurately simulated using the estimated parameters, as shown in Fig. 6(e).



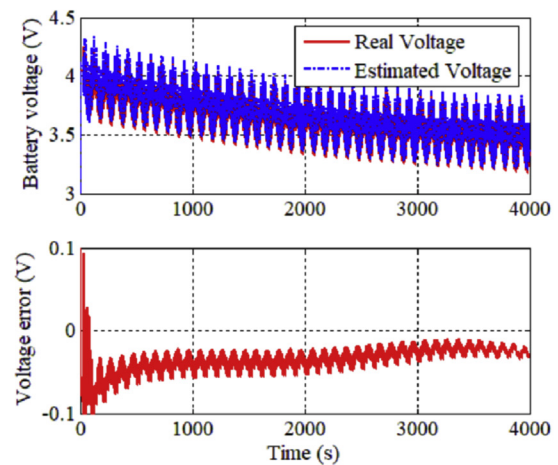
(a) Optimal current profile



(b) Parameters estimation result



(c) SoC estimation result



(d) v_b estimation result

Fig. 7. Experimental results of estimating all parameters/states simultaneously.

The proposed algorithm not only decreases the computational cost when compared to the case where all parameter/states are estimated simultaneously, but also improves estimation performance. This conclusion can be theoretically proven using Cramer-Rao (CR) bound analysis [51]. It has been shown that the estimation error is increased when more parameters are considered in the estimation [52]. Therefore, a single-parameter estimation is the most accurate as the least amount of uncertainty is involved in the estimation process. The proposed sequential algorithm can significantly improve the estimation accuracy when compared to multi-parameter estimation, given that the ECM voltage components can be separated [5]. Experiment #4 is conducted to verify the proposed sequential algorithm.

Experiment #4: Performance of the concurrent parameter/state estimation at 20 °C. The multi-scale EKF is used to estimate all parameters/states simultaneously [2,46]. When compared to the DEKF, the multi-scale EKF estimates parameters much slower than it estimates states because the parameters generally vary slowly [46]. An optimal current profile consisting of three sine waves (i.e., 0.01 Hz, 0.05 Hz, and 0.1 Hz) is used in Experiment #4, as shown in Fig. 7(a). Detailed information on determining these optimal current frequencies is provided in Ref. [52]. The parameter estimation results are shown in Fig. 7(b), revealing that the estimation performance of R_s and Q_b (i.e., SoH) are satisfactory. The estimated R_t and τ cannot track the actual values even using the optimal data, which can theoretically achieve the best estimation performance. As shown in Fig. 7(c), the estimated SoC needs a longer time to converge to the real value as compared to the sequential algorithm. Moreover, the static error of the estimated SoC is around 2%. The estimation error of the battery terminal voltage is correspondingly enlarged when more parameters are estimated, as shown in Figs. 4(f), 5(e), 6(e), and 7(d). Based on the above experimental results, it is shown that the sequential algorithm, which separates the estimation process, can achieve a better estimation performance when compared to the case where all parameters/states are estimated simultaneously. Since only a few parameters or states are estimated in each step, the estimation accuracy can be significantly improved.

We would like to point out that the implications of injecting a current signal for active parameter estimation could be complicated for general application (e.g., electric vehicles). However, an over-actuated system like the battery/supercapacitor (SC) hybrid energy storage system [53] or hybrid electric vehicle [54] provides an opportunity to inject desired signals for identification and achieve control objectives simultaneously [55]. Therefore, the proposed sequential algorithm can be directly used, and the potential negative influence of injecting the current on the system performance (i.e., system efficiency and power supply quality) can be minimized given the over-actuated nature. Specifically, for any power demand P_d , we have $P_d = P_{s1} + P_{s2}$, where P_{s1} and P_{s2} denote the power from source #1 (i.e., battery) and source #2 (i.e., SC). The required current for battery parameter/state estimation can be injected directly, while the SC can compensate to ensure the entire system supplies the demanded power. In addition, when the battery is used as the sole energy source, the proposed algorithm also can be used if the battery charging current can be changed and therefore the required excitation can be added. The influence of temperature is investigated in the experiment, and remarks are given to address the influence of battery degradation.

Remark 1. As a battery ages, its parameters will change, and the change will be reflected in the estimation results. One of the main goals for online parameter estimation is to detect aging for condition monitoring. It has been proven that the proposed sequential algorithm can accurately estimate battery parameters when they

change due to temperature and SoC variations. Therefore, the proposed algorithm can effectively detect the battery degradation in practical applications.

Another remark is given below to highlight the novelty of the proposed sequential algorithm when compared to existing methods.

Remark 2. As mentioned above, battery parameters vary with working conditions (e.g., temperature) and battery degradation levels. The results provided in Ref. [56] show promising experimental results for battery SoC and SoH estimation when the parameters can be calibrated offline and used online. However, it is challenging to calibrate battery parameters for all conditions (e.g., different temperatures and degradation levels). So an online method is still required for practical applications. When the battery is adopted in over-actuated systems, the proposed sequential algorithm can solve the aforementioned problem well by actively injecting persistently exciting signals, as shown in Figs. 4–6. It means that massive calibration is avoided by adopting the proposed algorithm, while the SoC/SoH estimation performance can still be ensured.

5. Conclusion

When battery states/parameters are estimated simultaneously, substantial uncertainties are introduced in the estimation process, and inaccurate parameters can therefore impair the state estimation performance. To this end, the sequential algorithm, which uses frequency-scale separation and estimates the parameters/states sequentially by injecting the current with different frequencies, is proposed in this paper. Specifically, by using a high-pass filter, the ohmic resistance R_s can be estimated independently via injecting a high-frequency current. Then, using the estimated R_s , the RC pair can be estimated by injecting a medium-frequency current. Finally, based on the above estimated parameters, the battery SoC and SoH can be estimated simultaneously. Experimental results show that the estimation accuracy of the proposed sequential algorithm is satisfactory and better than the case where all parameters/states are estimated simultaneously. The proposed algorithm can be implemented online when the battery is used in over-actuated systems. In future work, experiments under low SoH conditions will be conducted to further validate the effectiveness and robustness of the sequential algorithm, since it is generally challenging to guarantee state estimation accuracy under aged conditions.

Acknowledgement

This work is supported by the National Natural Science Foundation of China (Grant No. 51877057).

References

- [1] Ren H, Zhao Y, Chen S, Wang T. Design and implementation of a battery management system with active charge balance based on the SOC and SOH online estimation. *Energy* 2019;166:908–17.
- [2] Zhang C, Jiang J, Gao Y, Zhang W, Liu Q, Hu X. Charging optimization in lithium-ion batteries based on temperature rise and charge time. *Appl Energy* 2017;194:569–77.
- [3] Li X, Wang Z, Zhang L. Co-estimation of capacity and state-of-charge for lithium-ion batteries in electric vehicles. *Energy* 2019;174:33–44.
- [4] Feng S, Sun H, Zhang Y, Zheng J, Liu HX, Li L. Tube-based discrete controller design for vehicle platoons subject to disturbances and saturation constraints. *IEEE Trans Control Syst Technol* 2019.
- [5] Lin X, Stefanopoulou AG. Analytic bound on accuracy of battery state and parameter estimation. *J Electrochem Soc* 2015;162(9):A1879–91.
- [6] Gurjar M, Jalili N. Toward ultrasensitive mass detection using adaptive self-sensing piezoelectrically driven microcantilevers. *IEEE/ASME Trans*

- Mechatron 2007;12(6):680–8.
- [7] Ioannou PA, Sun J. Robust adaptive control, vol. 1. Upper Saddle River, NJ: PTR Prentice-Hall; 1996.
- [8] Zhang C, Allafi W, Dinh Q, Ascencio P, Marco J. Online estimation of battery equivalent circuit model parameters and state of charge using decoupled least squares technique. *Energy* 2018;142:678–88.
- [9] Çadırıcı Y, Özkazanç Y. Microcontroller-based on-line state-of-charge estimator for sealed lead–acid batteries. *J Power Sources* 2004;129(2):330–42.
- [10] Lin X, Perez HE, Mohan S, Siegel JB, Stefanopoulou AG, Ding Y, Castanier MP. A lumped-parameter electro-thermal model for cylindrical batteries. *J Power Sources* 2014;257:1–11.
- [11] Charkhgard M, Farrokhi M. State-of-charge estimation for lithium-ion batteries using neural networks and EKF. *IEEE Trans Ind Electron* 2010;57(12):4178–87.
- [12] Zou C, Hu X, Wei Z, Wik T, Egardt B. Electrochemical estimation and control for lithium-ion battery health-aware fast charging. *IEEE Trans Ind Electron* 2018;65(8):6635–45.
- [13] Wang Y, Zhang C, Chen Z. A method for state-of-charge estimation of Li-ion batteries based on multi-model switching strategy. *Appl Energy* 2015;137:427–34.
- [14] Hu X, Li S, Peng H. A comparative study of equivalent circuit models for Li-ion batteries. *J Power Sources* 2012;198:359–67.
- [15] Tang X, Wang Y, Zou C, Yao K, Xia Y, Gao F. A novel framework for Lithium-ion battery modeling considering uncertainties of temperature and aging. *Energy Convers Manag* 2019;180:162–70.
- [16] Rahimi-Eichi H, Baronti F, Chow MY. Online adaptive parameter identification and state-of-charge coestimation for lithium-polymer battery cells. *IEEE Trans Ind Electron* 2014;61(4):2053–61.
- [17] Zou Y, Hu X, Ma H, Li SE. Combined state of charge and state of health estimation over lithium-ion battery cell cycle lifespan for electric vehicles. *J Power Sources* 2015;273:793–803.
- [18] Gholizadeh M, Salmasi FR. Estimation of state of charge, unknown non-linearities, and state of health of a lithium-ion battery based on a comprehensive unobservable model. *IEEE Trans Ind Electron* 2014;61(3):1335–44.
- [19] Zheng Y, Ouyang M, Lu L, Li J, Zhang Z, Li X. Study on the correlation between state of charge and coulombic efficiency for commercial lithium ion batteries. *J Power Sources* 2015;289:81–90.
- [20] Plett GL. Extended Kalman filtering for battery management systems of LiPB-based HEV battery packs: Part 3. State and parameter estimation. *J Power Sources* 2004;134(2):277–92.
- [21] Sun F, Hu X, Zou Y, Li S. Adaptive unscented Kalman filtering for state of charge estimation of a lithium-ion battery for electric vehicles. *Energy* 2011;36(5):3531–40.
- [22] Kim IS. The novel state of charge estimation method for lithium battery using sliding mode observer. *J Power Sources* 2006;163(1):584–90.
- [23] Wang Y, Zhang C, Chen Z. A method for state-of-charge estimation of LiFePO₄ batteries at dynamic currents and temperatures using particle filter. *J Power Sources* 2015;279:306–11.
- [24] Zhu Q, Li L, Hu X, Xiong N, Hu GD. H_{∞} -Based nonlinear observer design for state of charge estimation of lithium-ion battery with polynomial parameters. *IEEE Trans Veh Technol* 2017;66(12):10853–65.
- [25] Rong P, Pedram M. An analytical model for predicting the remaining battery capacity of lithium-ion batteries. *IEEE Trans Very Large Scale Integr Syst* 2006;14(5):441–51.
- [26] He H, Xiong R, Zhang X, Sun F, Fan J. State-of-charge estimation of the lithium-ion battery using an adaptive extended Kalman filter based on an improved Thevenin model. *IEEE Trans Veh Technol* 2011;60(4):1461–9.
- [27] Wei Z, Zhao J, Ji D, Tseng KJ. A multi-timescale estimator for battery state of charge and capacity dual estimation based on an online identified model. *Appl Energy* 2017;204:1264–74.
- [28] Wang Z, Zeng S, Guo J, Qin T. State of health estimation of lithium-ion batteries based on the constant voltage charging curve. *Energy* 2019;167:661–9.
- [29] Meng J, Cai L, Stroe DI, Luo G, Sui X, Teodorescu R. Lithium-ion battery state-of-health estimation in electric vehicle using optimized partial charging voltage profiles. *Energy* 2019;185:1054–62.
- [30] Hu X, Yuan H, Zou C, Li Z, Zhang L. Co-estimation of state of charge and state of health for lithium-ion batteries based on fractional-order calculus. *IEEE Trans Veh Technol* 2018;67(11):10319–29.
- [31] Kim IS. A technique for estimating the state of health of lithium batteries through a dual-sliding-mode observer. *IEEE Trans Power Electron* 2009;25(4):1013–22.
- [32] Esfandyari MJ, Esfahanian V, Yazdi MH, Nehzati H, Shekoofa O. A new approach to consider the influence of aging state on Lithium-ion battery state of power estimation for hybrid electric vehicle. *Energy* 2019;176:505–20.
- [33] Ning B, Cao B, Wang B, Zou Z. Adaptive sliding mode observers for lithium-ion battery state estimation based on parameters identified online. *Energy* 2018;153:732–42.
- [34] Wan EA, Nelson AT. Dual extended Kalman filter methods. *Kalman filtering and neural networks*; 2001. p. 123–73.
- [35] Wang Y, Zhang C, Chen Z. A method for joint estimation of state-of-charge and available energy of LiFePO₄ batteries. *Appl Energy* 2014;135:81–7.
- [36] Lin X. Analytic analysis of the data-dependent estimation accuracy of battery equivalent circuit dynamics. *IEEE Control Syst Lett* 2017;1(2):304–9.
- [37] Song Z, Hou J, Xu S, Ouyang M, Li J. The influence of driving cycle characteristics on the integrated optimization of hybrid energy storage system for electric city buses. *Energy* 2017;135:91–100.
- [38] Weng C, Cui Y, Sun J, Peng H. On-board state of health monitoring of lithium-ion batteries using incremental capacity analysis with support vector regression. *J Power Sources* 2013;235:36–44.
- [39] Wang SL, Fernandez C, Zou CY, Yu CM, Li XX, Pei SJ, Xie W. Open circuit voltage and state of charge relationship functional optimization for the working state monitoring of the aerial lithium-ion battery pack. *J Clean Prod* 2018;198:1090–104.
- [40] Samad NA, Siegel JB, Stefanopoulou AG. Parameterization and validation of a distributed coupled electro-thermal model for prismatic cells. October. In: ASME 2014 dynamic systems and control conference. American Society of Mechanical Engineers; 2014. V002T23A006–V002T23A006.
- [41] Abu-Sharkh S, Doerffel D. Rapid test and non-linear model characterisation of solid-state lithium-ion batteries. *J Power Sources* 2004;130(1–2):266–74.
- [42] Guo Z, Qiu X, Hou G, Liaw BY, Zhang C. State of health estimation for lithium ion batteries based on charging curves. *J Power Sources* 2014;249:457–62.
- [43] Zhang C, Wang LY, Li X, Chen W, Yin GG, Jiang J. Robust and adaptive estimation of state of charge for lithium-ion batteries. *IEEE Trans Ind Electron* 2015;62(8):4948–57.
- [44] Hannan MA, Lipu MSH, Hussain A, Mohamed A. A review of lithium-ion battery state of charge estimation and management system in electric vehicle applications: challenges and recommendations. *Renew Sustain Energy Rev* 2017;78:834–54.
- [45] Lee JH, Ricker NL. Extended Kalman filter based nonlinear model predictive control. *Ind Eng Chem Res* 1994;33(6):1530–41.
- [46] Hu C, Youn BD, Chung J. A multiscale framework with extended Kalman filter for lithium-ion battery SOC and capacity estimation. *Appl Energy* 2012;92:694–704.
- [47] Haykin SS, editor. *Kalman filtering and neural networks*. New York: Wiley; 2001. p. 221–69.
- [48] Bt2000 battery testing system. Arbin Inc., Tech. Rep.; 2009.
- [49] Song Z, Hofmann H, Li J, Hou J, Zhang X, Ouyang M. The optimization of a hybrid energy storage system at subzero temperatures: energy management strategy design and battery heating requirement analysis. *Appl Energy* 2015;159:576–88.
- [50] Zhu JG, Sun ZC, Wei XZ, Dai HF. A new lithium-ion battery internal temperature on-line estimate method based on electrochemical impedance spectroscopy measurement. *J Power Sources* 2015;274:990–1004.
- [51] Rothenberger MJ, Docimo DJ, Ghanaatpishe M, Fathy HK. Genetic optimization and experimental validation of a test cycle that maximizes parameter identifiability for a Li-ion equivalent-circuit battery model. *J Energy Storage* 2015;4:156–66.
- [52] Song Z, Wu X, Li X, Hofmann H, Sun J, Hou J. Current profile optimization for combined state of charge and state of health estimation of lithium ion battery based on cramer-rao bound analysis. *IEEE Trans Power Electron* 2018;34(7):7067–78.
- [53] Song Z, Li J, Hou J, Hofmann H, Ouyang M, Du J. The battery-supercapacitor hybrid energy storage system in electric vehicle applications: a case study. *Energy* 2018;154:433–41.
- [54] Du J, Chen J, Song Z, Gao M, Ouyang M. Design method of a power management strategy for variable battery capacities range-extended electric vehicles to improve energy efficiency and cost-effectiveness. *Energy* 2017;121:32–42.
- [55] Reed DM, Sun J, Hofmann HF. Simultaneous identification and adaptive torque control of permanent magnet synchronous machines. *IEEE Trans Control Syst Technol* 2017;25(4):1372–83.
- [56] He H, Xiong R, Guo H. Online estimation of model parameters and state-of-charge of LiFePO₄ batteries in electric vehicles. *Appl Energy* 2012;89(1):413–20.